

Sweat Quantification During Electrodermal Analysis Combining Paper-Based Microfluidics with Printable Electrodes: Design and Materials

Batoul Hosseinzadeh¹^a, Sarah Tonello¹^b, Nicola Francesco Lopomo²^c and Emilio Sardini¹^d

¹Department of Information Engineering, University of Brescia, Via Branze, 38, Brescia, Italy

²Department of Design, Politecnico di Milano, Via Giovanni Durando, 10, Milano, Italy

Keywords: Electrodermal Activity, Paper-Based Microfluidics, Printable Electrodes, Microfluidic Systems.


Abstract: Significant challenges in Electrodermal Activity (EDA) are represented by poor wearability of commercial electrodes and imprecise differentiation between alterations in skin conductivity due to nervous system activities or sweat secretion in response to other stimuli. In this light, we propose a device that combines paper-based microfluidic with printable electrodes to monitor EDA and sweat rate/volume simultaneously. This setup not only refines wearability by implementing flexible, skin-compatible materials but also improves quantification accuracy by distinguishing between baseline EDA conductivity and actual sweat output providing a higher perception of the physiological state by harmonized sweat and EDA data. The preliminary analysis reported was performed in a laboratory environment aiming at two main objectives: i) optimize the design of paper-microfluidics pattern ii) compare different printable inks to select the most suitable one to minimize contact impedance and achieve a sensitivity comparable to standard EDA electrodes. Results obtained suggested the use of thick teeth design of microfluidics geometry to reduce variability in measurements and Poly(3,4-ethylenedioxythiophene) polystyrene sulfonate (PEDOT:PSS) as an optimal coating material to provide superior sensitivity (3.07 $\mu\text{S}/\mu\text{l}$) and repeatability (average Relative Standard Deviation (RSD) of 15%,) with a linearity range of 0-50 μl range while preserving low contact impedance and trustworthy signals.


1 INTRODUCTION


Wearable technologies have increasingly become popular, above all, in healthcare, since they allow to empower individuals by tracking their lifestyle and physiological conditions, timely (Iqbal, Mahgoub, Du, Leavitt, & Asghar, 2021). While most devices monitor physiological responses, such as pulse rate oxygen level or body temperature, new investigations concentrate on some valuable digital markers like Electrodermal Activity (EDA) as it represents an important tool in behavioral medicine, fulfilling as a biosignal for individual emotional response (both state and trait properties) (Chung et al., 2019; Kuo, Wu, & Wang, 2022); in fact, it directly tracks stress-related events on body activities and supports the definition of possible strategies to recover


psychosomatic conditions through biofeedback. Accurate EDA quantification is thus a crucial characteristic in developing wearable technology applicable in healthcare and occupational fields

In fact, EDA represents an effective solution in acquiring emotional and stress-related conditions, since its measurements is strictly related to complex physiological processes. In particular, physiological excitation is managed by a regulating interplay between the sympathetic and parasympathetic sectors of the autonomic nervous system (ANS); while the parasympathetic system preserve energy, the sympathetic part raises, metabolisms to tackle external provocation, enhancing heart rate, arterial pressure, and sweat secretion (Stanković, Adamec, Kostić, & Habek, 2021). Sympathetic fibrils enclose eccrine sweat secretors and their activation leads to

^a <https://orcid.org/0000-0002-0002-8172>

^b <https://orcid.org/0000-0002-7325-7988>

^c <https://orcid.org/0000-0002-5795-2606>

^d <https://orcid.org/0000-0001-8629-7316>

sweat production; as sweat penetrates the ducts, it generates low-resistance routes that amplify skin conductivity, detectable as electrodermal activity. EDA, therefore, represents sympathetic nervous functions and performs as a sensitive signal for alteration in excitement correlated to emotion, cognition, and awareness.

Clinically, EDA is tracked with an EDA sensor transcribes this conductivity alteration into analytical data (W. Boucsein, 2012). Although EDA measurement has proceeded during the past century, most research has been restricted to short-term observation in labs or distinct surroundings. There is an increasing demand for wearable technologies to track EDA over a long-term period, as they enable seamless and non-invasive data collection during daily activities (Kappeler-Setz, Gravenhorst, Schumm, Arnrich, & Tröster, 2013). This extended observation can disclose sympathetic nervous system patterns on a long-lived scale rather than short-term measurement, revealing states formerly unnoticeable. Additionally, monitoring EDA in “natural” and ecological conditions provides a more accurate and reliable understanding of physiological status than measurements in artificial settings (Posada-Quintero & Chon, 2020). However, a main challenge for pleasant long-term EDA recording is the limited accessibility of reliable and faithful flexible sensors. In fact, EDA measurement needs two electrodes, which must be placed on the user's skin; anyhow, present commercial silver/silver chloride (Ag/AgCl) electrodes are based on bulk materials and thence inflexible, and depend on gels and powerful adhesives, which can inhibit wearability, above all, whenever specific conditions are under analysis (W. Boucsein, 2012).

As wearable technology is growing, there are rising demands for flexible electrodes, requesting scalable manufacturing protocols (Zheng et al., 2014). Flexible and stretchable EDA sensors can be fabricated employing printed electrodes to present a novel technique that improves both the efficiency and convenience of wearable devices. Indeed, printed electrodes can be fabricated on flexible, and light substrates such as paper or polymers via scalable approaches such as inkjet or screen printing, which are economical and authorized for faithful patterning (Pang, Lee, & Suh, 2013). With printed electrodes, EDA sensors can be effectively integrated into wearable tools, embedded into clothing, or attached directly to the skin, providing continuous and seamless tracking of emotional and stress-related states in real-world conditions. Moreover, printed electrodes promote higher sensitivity and versatility, necessary for recording narrow alterations in skin

conductivity associated with stress and excitement. This development not only expands the implementation of EDA measurement in health and behavioral research but also assists the development of effective and user-friendly wearable technology.

Additionally, EDA sensors clinically encounter some restrictions due to their inability to precisely differentiate between alterations in skin conductivity related either to true sweat secretion or other environmental parameters. These variations result in inherent variability in EDA monitoring, specifically during long-term tests, where evaporation and weak adherence influence signal trustworthiness (Cui & Schlessinger, 2006). Incorporating a microfluidic system overcomes these limitations by transferring sweat continually to the electrodes, preserving acceptable skin contact and minimizing dehydration-related attenuation. On the other hand, microfluidic channels, been fabricated for this purpose, could allow to obtain also accurate sweat rate and volume measurements, acquired in parallel to EDA data, thus serving to distinguish between baseline conductance alterations and real sweat events (Ullah et al., 2023). While conventional microfluidic devices require complicated lithographic operations, hydrophilic porous channels like filter paper turned up as an easier substitute; in fact, the paper-based apparatus utilizes natural capillary movement to instantly take in and transfer sweat, enabling them efficient for constant, skin-compatible observation (Silva-Neto et al., 2023).

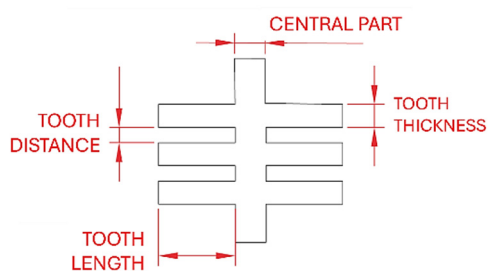
In this study, we propose a novel integrated solution able to simultaneously track the electrodermal activity and sweat rate employing a unified electrode design. The sensor under development combines a paper-based microfluidic system with printed electrodes to monitor both EDA and sweat rate/volume. This multi-functional action can provide accurate measuring of skin conduction alteration while steadily collecting and evaluating sweat along the microfluidic layer. The paper-based absorptive layer conducts sweat instantly from the skin to the electrodes, enabling immediate measuring of sweat secretion rate and volume. This setup not only refines wearability through the implementation of flexible, and skin-compatible materials but also improves quantification accuracy by distinguishing between baseline EDA conductivity and actual sweat output providing a higher perception of the physiological state by harmonized sweat and EDA data. In this picture, the present contribute reports a preliminary analysis of the design in term of paper-microfluidics geometry and of printable materials to maximize flexibility and to minimize contact impedance.

2 MATERIALS AND METHODS

The materials employed for preparing the paper-based microfluidic sensor included: Whatman filter paper (Grade 1), chosen for fast fluid transportation of 150 sec/100 ml, Poly(3,4-ethylenedioxythiophene) polystyrene sulfonate (PEDOT:PSS) and single-walled Carbon nanotube (CNT); phosphate buffer solution (PBS) (pH: 7.4); all these materials were purchased from Sigma Aldrich company. The disposable Ag/AgCl conductive hydrogel EDA Electrodes were obtained from Cardinal Health™. Silver nanoparticles based aqueous ink (JS-A426) was obtained from Novacentrix.

2.1 Layout Design

The geometry design of the microfluidic system is important for effective sweat delivery and in line with EDA signal recording. The patterns were designed using a standard CAD software (Autocad) to investigate the optimal route for fluid flow through the Whatman paper by exploiting capillary action, and to guarantee that liquid was delivered to the electrodes without untimely dehydration. Each structure concentrated on designing an adjusted, small pathway to conduct liquid correctly from input to the sensing electrodes. The branched pattern structure was utilized to assess equal distribution, which enhances the sensitivity and stability of the signal. Thence, patterns in four different configurations were designed, with dimensions of central part, thickness tooth, distance, and length tooth as detailed in figure 1.



Configuration name	Central part (mm)	Tooth thickness (mm)	Tooth distance (mm)	Tooth length (mm)
Short thin	4	2	3	6
Short thick	4	3	2	6
Long thin	4	2	3	10
Long thick	4	3	2	10

Figure 1: Details of paper microfluidics patterns.

2.2 Laser-Cut Microfluidics Pattern

The preparation of the paper-based microfluidic pattern was carried out by using a CO₂ laser cutting system (FLUX Beambox instrument, 40 W laser and 1000 dpi resolution). Cutting parameters were defined compatible with Whatman filter paper to avoid extra heating buildup; specifically, the precise defined designs were introduced into the cutter software (Beam Studio) and critical parameters, such as power, speed, and frequency, were attentively calibrated to obtain clean, slight channels without burning or damaging the paper edges. Eventually, a medium power of 18 % of maximum output and a mild cutting speed of 18 mm/s were set to keep the paper's structural unity and capillary features.

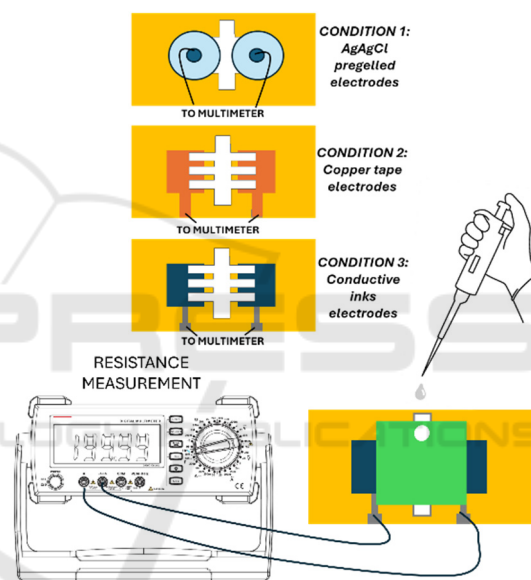


Figure 2: Experimental set up.

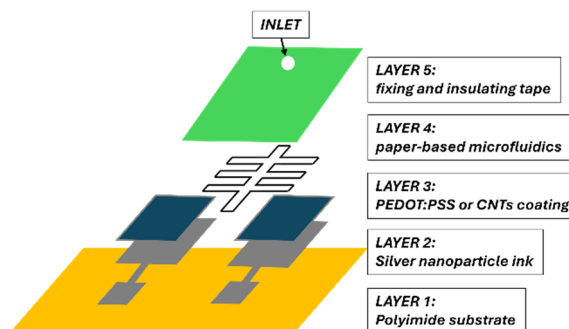


Figure 3: Detailed components of the devices combining printed approach to realize EDA with microfluidics.

2.3 Measurement Protocol

The protocol for characterizing electrodes exploited the use of a controlled volume of a PBS solution to induce measurable changes in the DC resistance, from which changes in conductance can be then calculated as the reciprocal of the values obtained. The instrument employed to perform measurement was a benchtop digital multimeter (6 1/2 digits, Keysight) with a sampling rate of 2 Hz. This PBS saline solution was selected to imitate sweat owing to its comparable ionic constitution. The relation between volume and resistance was obtained by performing following standard addition of 10 μ l injected into the inlet part of the paper-based microfluidic pattern. Three different types of electrodes were compared. The traditional EDA Ag/AgCl pre-gelled wet electrodes were examined first to monitor their feedback to the conductive way generated by the liquid (condition 1, fig. 2). Further, two different configurations with dry electrodes were tested: dry copper tape electrodes and dry electrodes realized with different combinations of printable inks (condition 2 and 3, fig. 2).

The copper electrodes, introduced as a first step to simulate dry printed electrode configuration, were obtained by cutting the conductive copper tape into 1.5 cm \times 1.5 cm dimensions and located underneath the paper-based microfluidic structure, setting up a conductive medium for initial conduction measuring. This copper-tape-based layout lets us evaluate a dry electrode-based setup and improve the protocol.

A similar construction was assembled using the printed electrode approach. A 1.5 cm \times 1.5 cm area was covered with a layer of silver ink to make a firm and highly conductive foundation. To improve and optimize signal sensitivity and reduce contact impedance, a secondary conductive film was coated on top of the silver base, made of either PEDOT:PSS or CNT, materials well-known for their flexibility and conductivity (figure 3). Every setup (copper tape, Ag/PEDOT:PSS, and Ag/CNT) was specifically examined, by individually exploiting the same procedure (figure 2). Variability and repeatability were evaluated by replicating the same measurements in different conditions; repeatability, in particular, was evaluated replicating each test for at least four times for any electrode composition. Furthermore, reproducibility was evaluated by preparing 3 identical configurations for each material type and repeating the test.

2.4 Data Analysis

Data obtained from each resistance measurement against time were converted in conductivity values by calculating the reciprocal of the DC resistance. After that, data were filtered with a moving-average filter (window of 20 samples), to remove high-frequency noise before proceeding with the calculation of metrological parameters. Further, median filters were exploited to remove spikes due to external interference during the following injections.

Conductivity values used to build the calibration plot were sampled from the measured curve against time exploiting a thresholding of the first derivative of the signal. In detail, injection times were recognized on the plot as the instants corresponding to the values overcoming a defined threshold; the threshold was adapted depending on the full-scale range measured in each test. Once the injection times were identified, sampling times were detected adding 30 s to each injection time, and the conductivity value corresponding to that instant was sampled and exploited to build the calibration curve. The 30 s delay of the sampling time respect to the injection time allow us to properly sample conductivity values after that transient behavior occurring at every injection. This transient instability observed for the first seconds after each injection represents a well-known challenge when coupling electrodes with microfluidics (Arantes & Paixão, 2022; Lai, Lim, Lee, & Huang, 2021) and it is due to the perturbation of the complex interaction between paper-based microfluidics surface and conductive electrodes taking place when the newly injected liquid is filling the porous microfluidics, thus they should not be considered since in those instants the proportionality between liquid volume and conductivity does not appear well defined.

Sensitivity was calculated as the slope of the calibration curve obtained by fitting the current values corresponding to each concentration. Relative Standard Deviation (RSD) was also calculated as the ratio between the standard deviation and the average value of repetitive measurements.

3 RESULTS

3.1 Geometries Comparison

Results obtained from experiments carried out using wet electrodes to compare different geometries of the laser-cut paper-based layouts showed no significant differences in terms of sensitivities, as summarized in

Table 1 and displayed graphically in figure 4. Thus, despite the short-thin-teeth geometry showed the highest average sensitivity, the high RSD associated made this approach worst compared with other geometries.

Table 1: Average sensitivities in $\mu\text{S}/\mu\text{L}$ obtained for each geometry, and corresponding RSD in %.

Geometry	Sensitivity ($\mu\text{S}/\mu\text{L}$)	Max RSD (%)
Short Thin	2.629	46%
Long Thin	1.699	21%
Short Thick	2.241	13%
Long Thick	2.162	15%

Significant differences can be observed in terms of variabilities. Thin-teeth geometries in particular showed relative standard deviations higher than 30% for short and 15% for long teeth. On the contrary, thick teeth both long and short, showed comparable variabilities, lower than 15% for all the volumes of PBS tested (figure 5).

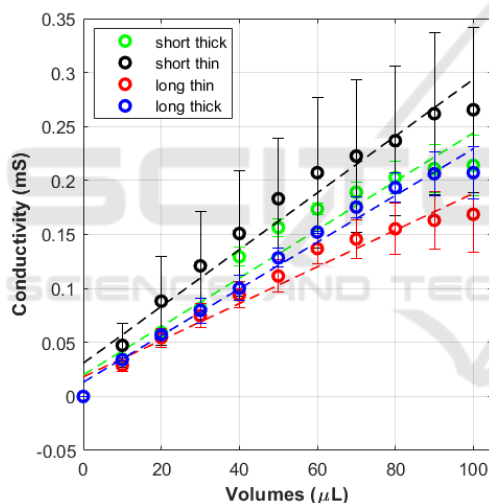


Figure 4: Comparison among calibration curves obtained combining pre-gelled Ag-AgCl electrodes with different paper-based laser cut designs.

This difference should probably be due to the most stable contact area created between the pattern and electrodes in the case of thicker than thinner teeth. Further, the higher available surface provides an increased absorption capacity during the different steps. Considering these results, since lower RSD in the studies indicates a higher reliable measurement system, crucial for accurate process improvement, thick teeth geometries were selected as the most reliable for further tests.

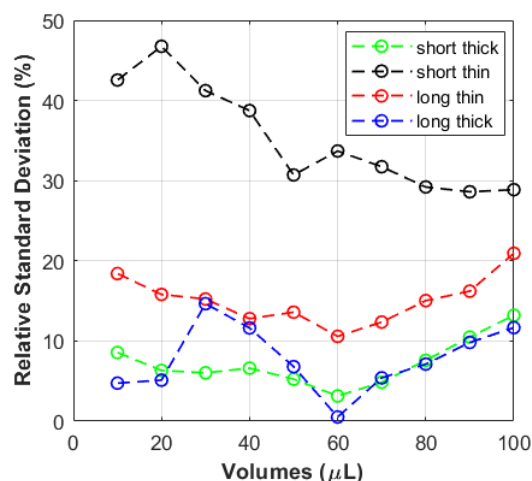


Figure 5: Comparison among RSD obtained combining pre-gelled AgAgCl electrodes with different paper-based laser cut designs.

3.2 Wet and Dry Electrodes Comparison

Significant differences can be observed comparing the traditional pre-gelled wet electrodes in Ag/AgCl with the dry copper electrodes, with no significant differences between the geometry with long teeth and the one with short teeth. The similarity observed between long and short teeth represents an interesting finding that provides the opportunity to adapt the length of the teeth in future works targeting simultaneous sweat volume and EDA measurements. The teeth length can therefore be optimized depending on the distance between the electrodes that can ensure the most suitable EDA measurements. Considering that, from literature, the most common distances between EDA electrodes is between 10 and 20 mm, long teeth geometry appears as the most promising and thus the experiments performed employing printable inks were performed relying on this geometry. Results obtained in terms of sensitivities, linear ranges, and RSD are summarized in Table 2 and graphically shown in figure 6.

Table 2: Average sensitivities in $\mu\text{S}/\mu\text{L}$ obtained for the two different electrode types (wet and dry), and corresponding RSD in %.

Electrode type	Geometry	Range linearity (μL)	Sensitivity ($\mu\text{S}/\mu\text{L}$)	Max RSD (%)
WET	Short Thick	0-100	2.403	21%
WET	Long Thick	0-100	2.420	18%
DRY	Short Thick	0-50	0.518	50%
DRY	Long Thick	0-50	0.433	50%

In particular, regarding the sensitivities, wet electrodes showed an average sensitivity of almost 5 fold respect to dry copper electrodes, in the range 0-50 μL , and of almost 25-fold in the range 50-100 μL where the dry electrodes showed a saturation behaviour, with a sensitivity of $0.1 \pm 0.01 \mu\text{S}/\mu\text{L}$. Regarding variability, the largest variability was observed in the range 0-50 μL , where dry electrodes showed RSD higher than 50%. This behaviour could be related to a limited interface between the dry electrode surface and the paper surface poorly soaked in PBS. The RSD appears to decrease, reaching values comparable with the wet-gelled electrodes for volumes in the range 50-100 μL , where probably a higher surface interaction is obtained due to the increased soaking of the paper fluidics. Differently from dry electrodes, wet electrodes showed similar RSD ($< 20\%$) for all the volumes of PBS injected, regardless of the range tested, confirming that the gelled surfaces of the electrodes ensure a lower contact impedance and a stable interface with the

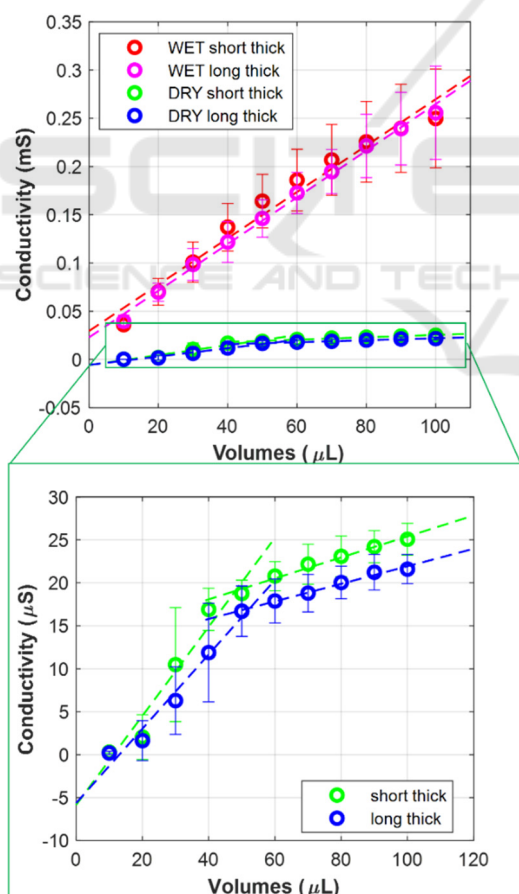


Figure 6: Comparison among calibration curves obtained employing wet and dry electrodes combined with thick-teeth pattern geometries.

paper fluidics no matter the level of paper soaking. The significant differences observed in this comparison, in terms of both sensitivity and variability, raise relevant discussion points regarding the type of material that needs to be used to guarantee low contact impedance and stable interface between paper and electrode. Following several literature evidence, the choice of the material was thus addressed to nanomaterials and conductive polymers (e.g. PEDOT:PSS) both well-known to improve contact impedance issues traditionally emerging when dealing with dry electrodes.

3.3 Ink Combinations Comparison

A significant increase in terms of sensitivity could be obtained by relying on both CNT and PEDOT:PSS coatings, with respect to bare silver electrodes, as it can be observed from the comparison among the measured curves reported in Figure 7. Examples of measurements obtained during repeatability and reproducibility tests are reported in Figures 8 and 9. A summary of sensitivity and RSD in each single run and the averaged values across different electrodes (reproducibility test) and different repetitions of the measurements on the same electrodes (repeatability tests) can be summarized in Tables 3 and 4. Results reported focus only on the range 0-50 μL to exclude higher volume for which both CNTs and PEDOT:PSS coated electrodes showed saturation.

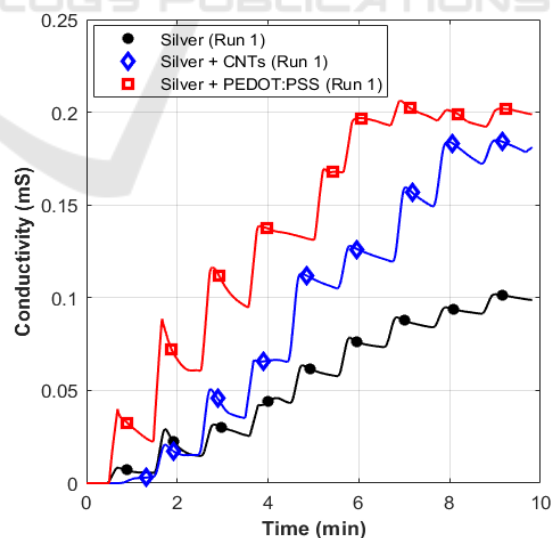


Figure 7: Comparison among conductivity measurements obtained combining long-thick-teeth pattern geometry with three different combinations: silver, silver + CNTs, silver + PEDOT:PSS.

For all the conditions tested during the repeatability test, measurements performed after the first showed a decrease in sensitivity, consequent to changes in the surface contact interface happening after the first contact between PBS, paper, and the conductive surface of the electrode. Electrodes realized using silver coated with PEDOT:PSS however showed a higher repeatability compared to silver and silver coated with carbon nanotubes, with an RSD ranging from 6 to 14 %. As a negative aspect, as it can be observed from Figure 5, PEDOT:PSS showed a smaller linearity range, with a saturation after 50 μl . This result should be kept under consideration especially if targeting applications with high sweat rates; in this specific case, a solution might be to employ a paper with a higher absorption capacity to extend the linearity range of measurements. Regarding the reproducibility test, silver electrodes showed the best results, with RSD lower than 10 %. The higher RSD obtained for coated electrodes (<30% for CNTs and <22% for PEDOT:PSS) can be explained by considering the variability of the additional layer of ink deposited on top of silver. Similarly to the measurements reported for the repeatability test, even in Figure 6, it can be

appreciated that PEDOT:PSS performs better than the other only in the range 0-50 μl , showing worse reproducibility outside that range.

Table 3: Summary of the results from the repeatability test, given as average sensitivities in $\mu\text{S}/\mu\text{l}$ and RSD in % obtained for each replicate of the electrodes (A, B, C, D) on three repeated measurements on the same electrodes.

Electrodes	Metrological characteristics	Ag	Ag + CNTs	Ag + PEDOT
ELE A	sensitivity ($\mu\text{S}/\mu\text{l}$)	1.14	1.40	3.57
	RSD %	56	41	6
ELE B	sensitivity ($\mu\text{S}/\mu\text{l}$)	1.21	1.77	2.59
	RSD %	53	67	9
ELE C	sensitivity ($\mu\text{S}/\mu\text{l}$)	1.08	1.33	3.24
	RSD %	54	58	5
ELE D	sensitivity ($\mu\text{S}/\mu\text{l}$)	1.10	2.11	2.76
	RSD %	53	74	14

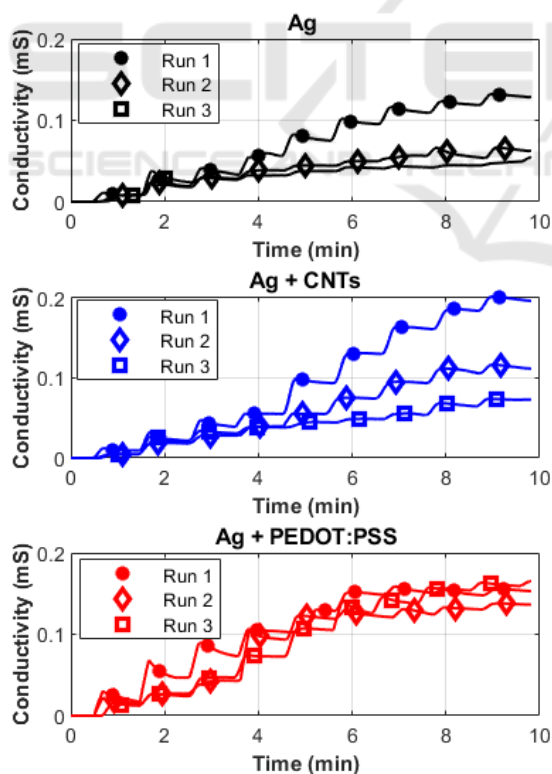


Figure 8: Examples of repeatability tests on different ink combinations: on each electrode couple the same measurement was repeated three times.

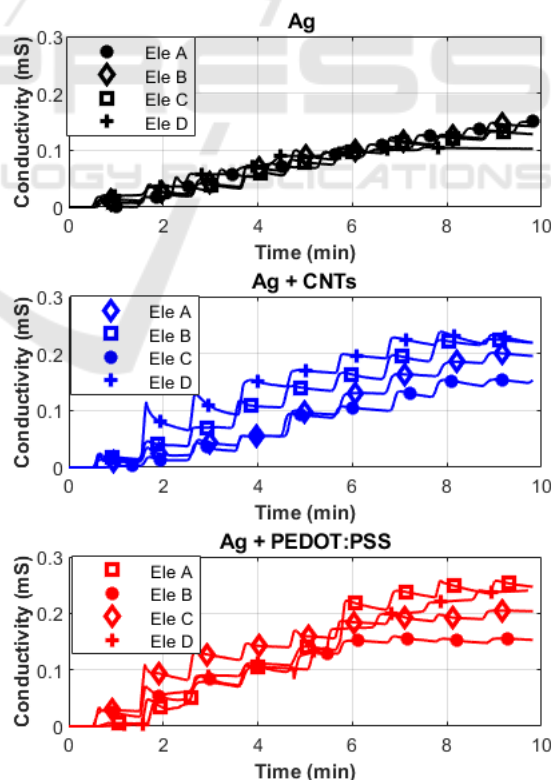


Figure 9: Examples of reproducibility tests on different ink combinations: the same measurement was performed on four different replicates of electrode couples.

Table 4: Summary of the results from the reproducibility test, given as average sensitivities in $\mu\text{S}/\mu\text{l}$ and RSD in % obtained for each run on four different replicates of the EDA conductive electrodes combined with microfluidic path.

Run Number	Metrological characteristics	Ag	Ag + CNTs	Ag + PEDOT
RUN 1	sensitivity ($\mu\text{S}/\mu\text{l}$)	1.82	2.80	3.07
	RSD (%)	5	30	11
RUN 2	sensitivity ($\mu\text{S}/\mu\text{l}$)	0.89	1.29	3.14
	RSD (%)	8	25	16
RUN 3	sensitivity ($\mu\text{S}/\mu\text{l}$)	0.68	0.87	2.91
	RSD (%)	10	9	22

Overall, considering a trade-off among sensitivity, repeatability, and reproducibility PEDOT:PSS appear as the most suitable material to realize electrodes for electrodermal activity combined with paper-based microfluidics to monitor sweat volume. The sensitivity obtained for PEDOT:PSS coated silver electrodes, with an average of $3.07 \mu\text{S}/\mu\text{l}$ and an average RSD of 15%, represents high promising results if compared with the one obtained with standard pre-gelled wet electrodes, with an average of $2.4 \mu\text{S}/\mu\text{l}$ and an average RSD of 20%.

4 CONCLUSIONS

This study focused on microfluidic pattern design and electrode materials selection for EDA and sweat rate monitoring and highlighted the need for performance trade-offs. The thick-teeth geometry demonstrated the most faithful structure for paper-based microfluidics, certifying lower variability through stable electrode contact. To reduce the gap between wet and dry electrodes and surpass the limitations of the dry electrode in terms of sensitivity and consistency PEDOT:PSS electrodes provided better results than the other studied materials since it displayed superior sensitivity and repeatability within the $0\text{-}50 \mu\text{l}$ range while preserving low-contact impedance and trustworthy signals. Future works may concentrate on the evaluation of different printing techniques to realize the overall device and on the enhancement of absorption volume to increase linearity and establish powerful performance across a wide range of various conditions (e.g. volume and rate ranges).

ACKNOWLEDGEMENTS

This study was carried out within the MICS (Made in Italy – Circular and Sustainable) Extended Partnership and received funding from Next-GenerationEU (Italian PNRR – M4 C2, Invest 1.3 – D.D. 1551.11-10-2022, PE00000004 CUP D73C22001250001).

REFERENCES

- Arantes, I. V. S., & Paixão, T. R. L. C. (2022). Couple batch-injection analysis and microfluidic paper-based analytical device: A simple and disposable alternative to conventional BIA apparatus. *Talanta*, *240*, 123201. doi:10.1016/j.talanta.2021.123201
- Chung, H. U., Kim, B. H., Lee, J. Y., Lee, J., Xie, Z., Ibler, E. M., ... Rogers, J. A. (2019). Binodal, wireless epidermal electronic systems with in-sensor analytics for neonatal intensive care. *Science*, *363*(6430). doi:10.1126/science.aau0780
- Cui, C.-Y., & Schlessinger, D. (2006). EDA Signaling and Skin Appendage Development. *Cell Cycle*, *5*(21), 2477–2483. doi:10.4161/cc.5.21.3403
- Iqbal, S. M. A., Mahgoub, I., Du, E., Leavitt, M. A., & Asghar, W. (2021). Advances in healthcare wearable devices. *Npj Flexible Electronics*, *5*(1), 9. doi:10.1038/s41528-021-00107-x
- Kappeler-Setz, C., Gravenhorst, F., Schumm, J., Arnrich, B., & Tröster, G. (2013). Towards long term monitoring of electrodermal activity in daily life. *Personal and Ubiquitous Computing*, *17*(2), 261–271. doi:10.1007/s00779-011-0463-4
- Kuo, W.-C., Wu, T.-C., & Wang, J.-S. (2022). Design and Application of a Flexible Blood Oxygen Sensing Array for Wearable Devices. *Micromachines*, *13*(10), 1742. doi:10.3390/mi13101742
- Lai, Y.-H., Lim, J.-C., Lee, Y.-C., & Huang, J.-J. (2021). Analysis of the Biochemical Reaction Status by Real-Time Monitoring Molecular Diffusion Behaviors Using a Transistor Biosensor Integrated with a Microfluidic Channel. *ACS Omega*, *6*(18), 11911–11917. doi:10.1021/acsomega.1c00222
- Pang, C., Lee, C., & Suh, K. (2013). Recent advances in flexible sensors for wearable and implantable devices. *Journal of Applied Polymer Science*, *130*(3), 1429–1441. doi:10.1002/app.39461
- Posada-Quintero, H. F., & Chon, K. H. (2020). Innovations in Electrodermal Activity Data Collection and Signal Processing: A Systematic Review. *Sensors*, *20*(2), 479. doi:10.3390/s20020479
- Silva-Neto, H. A., Arantes, I. V. S., Ferreira, A. L., do Nascimento, G. H. M., Meloni, G. N., de Araujo, W. R., ... Coltro, W. K. T. (2023). Recent advances on paper-based microfluidic devices for bioanalysis. *TrAC Trends in Analytical Chemistry*, *158*, 116893. doi:10.1016/j.trac.2022.116893

- Stanković, I., Adamec, I., Kostić, V., & Habek, M. (2021). Autonomic nervous system—Anatomy, physiology, biochemistry (pp. 1–17). doi:10.1016/bs.irmvd.2021.07.006
- Ullah, H., Shoaib, F., Zahid, S. D., Mahmood, M. I., Ali, M., Ali, M., ... Jafry, A. T. (2023). *Design and Fabrication of Digital Microfluidics device for Lab-on-a-Chip Applications*. In *ICAME 2023* (p. 7). Basel Switzerland: MDPI. doi:10.3390/engproc2023045007
- W. Boucsein. (2012). *Electrodermal Activity*. USA:Springer,.
- Zheng, Y.-L., Ding, X.-R., Poon, C. C. Y., Lo, B. P. L., Zhang, H., Zhou, X.-L., ... Zhang, Y.-T. (2014). Unobtrusive Sensing and Wearable Devices for Health Informatics. *IEEE Transactions on Biomedical Engineering*, 61(5), 1538–1554. doi:10.1109/TBME.2014.2309951

